AIAA'83

# AIAA-83-0236
# Three-Dimensional Euler Equation Simulation of Propeller-Wing Interaction in Transonic Flow

D.L. Whitfield, Mississippi State Univ., Mississippi State, MS; and A. Jameson, Princeton Univ., Princeton, NJ

**AIAA 21st Aerospace Sciences Meeting**

January 10-13, 1983/Reno, Nevada

# THREE-DIMENSIONAL EULER EQUATION SIMULATION OF PROPELLER-WING INTERACTION IN TRANSONIC FLOW*

D. L. Whitfield†
Department of Aerospace Engineering
Mississippi State University
Mississippi State, MS 39762

and

A. Jameson††
Department of Mechanical and Aerospace Engineering
Princeton University
Princeton, N. J. 08544

## Abstract

A method is presented for the computation of propeller-wing interaction in transonic rotational flow. The approach is to use the three-dimensional time-dependent Euler equations with force terms included to simulate the propeller. Viscous-inviscid interaction on the wing surface is included by coupling the three-dimensional Euler equations with the two-dimensional compressible turbulent inverse integral boundary-layer equations. Numerical solutions are compared with experimental data for a 32° swept supercritical wing without a propeller simulator, wing with a propeller simulator producing thrust only, and wing with a propeller simulator producing thrust and swirl in each direction.

## I. Introduction

Studies indicate that a significant reduction in fuel consumption of transport aircraft can be achieved by advanced technology turboprop or propfan propulsion systems. It is intended that such propulsion systems be used on transonic aircraft. Small changes in transonic flow about a wing can cause appreciable change in shock wave strength and location, and consequently influence lift, drag, boundary-layer growth, separation, etc. Because propellers can produce significant changes in the transonic flow about a wing, it is necessary to understand the influence of a propeller slipstream on a supercritical type wing. The purpose of this paper is to present a computational fluid dynamic method of simulating three-dimensional transonic propeller-wing interaction, including swirl.

Most investigations of propeller-wing flowfields have been limited to subsonic[1-5] and high subsonic[6] Mach numbers. Rizk[7] and Narain[8] have investigated the transonic problem using the potential flow equations. A transonic propeller-wing interaction flowfield, however, is rotational due to variations in flow properties induced by the propeller, embedded shocks, and viscous effects. The approach taken in this work is to use the three-dimensional time-dependent Euler equations, including the energy equation, in order to allow for rotational flow. In addition, viscous effects are taken into account by coupling the three-dimensional Euler equations with the two-dimensional compressible turbulent inverse integral boundary-layer equations.

*This research was sponsored by the Lockheed-Georgia Company, Marietta, GA.
†Professor, Member AIAA.
††Professor.

The method used to incorporate the influence of a propeller in the Euler equations is described in the following section. The Euler equation solver is then briefly discussed followed by an explanation of how viscous-inviscid interaction is included in the computational metod. Finally numerical results are presented and compared with results from a transonic flow experiment designed to simulate the influence of a propeller on a supercritical wing.

## II. Propeller Simulation

The integral form of the Euler equations is used in the present work. From these conservation law equations of mass, momentum, and energy, certain jump conditions can be derived for discontinuity surfaces.[9] One of the discontinuity surfaces permitted is a shock, across which there is mass flow. Shocks can be captured in the solution. Another discontinuity surface permitted is one whereby there is no mass flow across the surface. For this latter discontinuity surface, the jump in tangential velocity and density across the surface are arbitrary but the jump in pressure is zero. A jump in energy is permitted although the jump must satisfy an equation of state.[10] Such jump conditions include those necessary to resolve a propeller slipstream. Assuming the method of incorporating the influence of the propeller in the Euler equations is adequate (to be explained below) the approach is to capture the slipstream in the solution as opposed to modeling it explicitly.

The method used to incorporate the influence of the propeller in the Euler equations is as follows. Forces operate on the fluid as a consequence of the lift and drag of the blades as illustrated in Fig. 1. Because the numerical formulation of the Euler equations used here is finite volume, the forces of the blades on the fluid become force vectors associated with the finite volumes located in the propeller region (Fig. 1). These finite volume force vectors are variable due to propeller rotation, blade twist, etc.

If these finite volume force vectors had resulted from the usual concept of a body force per unit mass, $\vec{f}$, such as gravitational or electromagnetic forces, then the three-dimensional time-dependent Euler equations could be written in cartesian coordinates for a stationary grid as

$$\int_{V_o} \frac{\partial \vec{G}}{\partial t}\, dV + \int_{S_o} (\vec{F}_x n_x + \vec{F}_y n_y + \vec{F}_z n_z)\, dS - \int_{V_o} \vec{B}\, dV = 0 \tag{1a}$$

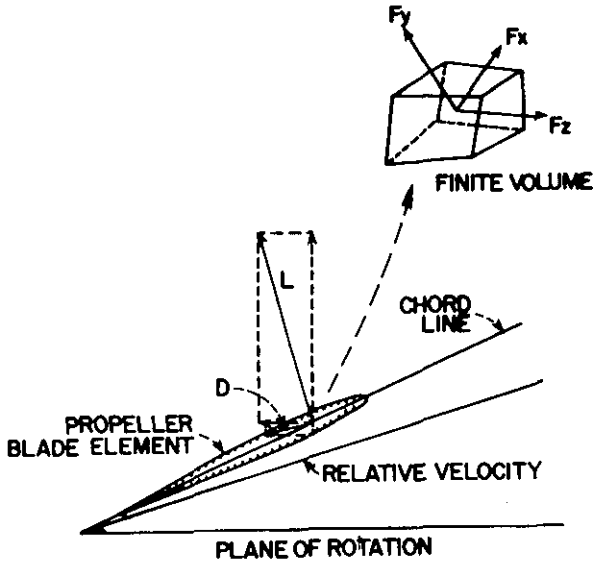


Fig. 1 Force Diagram of a Propeller Blade Element

where

$$\vec{G} = [\rho,\ \rho u,\ \rho v,\ \rho w,\ \rho E]^T \tag{1b}$$

$$\vec{F}_x = [\rho u,\ \rho uu+p,\ \rho vu,\ \rho wu,\ \rho(E+p/\rho)u]^T \tag{1c}$$

$$\vec{F}_y = [\rho v,\ \rho uv,\ \rho vv+p,\ \rho wv,\ \rho(E+p/\rho)v]^T \tag{1d}$$

$$\vec{F}_z = [\rho w,\ \rho uw,\ \rho vw,\ \rho ww+p,\ \rho(E+p/\rho)w]^T \tag{1e}$$

$$\vec{B} = [0,\ \rho f_x,\ \rho f_y,\ \rho f_z,\ \rho(f_x u + f_y v + f_z w)]^T \tag{1f}$$

$$E = \frac{p}{\rho(\gamma-1)} + \frac{1}{2}(u^2 + v^2 + w^2) \tag{1g}$$

and $n_x$, $n_y$ and $n_z$ are the x, y, z components of the outward unit normal vector on the surface S enclosing the volume $V_o$. By applying Eq. (1a) to each volume, the result of the integral of $\vec{B}$ would be a force vector at each cell (finite volume). To account for the effect of a propeller, the cell forces per unit volume are replaced by an eqivalent stress system composed of forces per unit area exerted on the cell faces. This concept has similarities to that used in magnetohydrodynamics with regard to Maxwell stresses (see e.g. Shercliff[11]). Therefore, because numerical discretization of the last term in Eq. (1a) at each cell results in a force in each of the three momentum equations, and each component of force multiplied by the corresponding component of velocity in the energy equation, the influence of the propeller on the flow is regarded as a force per unit area (stress) applied to the cell faces, and numerical treatment of a surface integral rather than a volume integral results in forces occurring in the Euler equations in the same manner as body forces. The last term on the left hand side of Eq. (1a), therefore, is written in terms of a stress system using Gauss' divergence theorem as

$$\int_{V_o} \vec{B} dV = \int_{V_o} \text{div}\ \vec{\tau} dV = \int_{S_o} \vec{\tilde{B}} dS \tag{2}$$

where

$$\vec{\tilde{B}} = \vec{\tau} \cdot \vec{n} = [0,\ \tilde{f}_x,\ \tilde{f}_y,\ \tilde{f}_z,\ \tilde{f}_x u + \tilde{f}_y v + \tilde{f}_z w]^T \tag{3}$$

and $\vec{\tilde{f}}$ is a force per unit area.

Information necessary to specify the stress vector $\vec{\tilde{f}}$ might be obtained from the propeller characteristics. The available experimental transonic flow data of Wedge and Crowder,[12] however, were obtained using a simulator to investigate the effects of a propeller on a supercritical wing. Total pressure jumps were introduced by the simulator and vanes were used to induce swirl. The thrust was, therefore, imposed in the present computations by introducing the same jump in total pressure as used in the experiments. The force components in the plane perpendicular to the thrust were adjusted to provide the swirl velocities induced by the simulator vanes. This was necessary because swirl velocities are not imposed in the computations, rather they are obtained as part of the solution. A variation in the stress vector, $\vec{\tilde{f}}$, proportional to the square of the distance from the center of the propeller (or simulator in this case) was used to more appropriately simulate spatial variations.

## III. Euler Equations Solver

The method used to solve the three-dimensional time-dependent Euler equations with force terms is an extension of that described in Ref. 13. Finite volume spatial discretization is applied to the integral form of the Euler equations and the resulting equations are solved using a four-stage two-level numerical scheme. The four-stage scheme used is second-order accurate whereas the four-stage scheme used in Ref. 13 was fourth-order accurate. The second-order scheme is used because it requires slightly less storage than the fourth-order scheme and, also, steady state solutions are of interest as opposed to time accurate solutions.

Dissipative terms are introduced in this central difference scheme in a separate filter stage at the end of each time step. Convergence to a steady state is accelerated by the addition of a forcing term that depends on the difference between the local total enthalpy and the freestream value of enthalpy. Convergence is also accelerated by using a local time step determined by the maximum Courant number of $2\sqrt{2}$. Far field boundary conditions are based on a characteristic combination of variables.[13] Pressure at the wall is determined by a three-dimensional version of the work of Rizzi[14] involving the normal momentum relation.

## IV. Viscous-Inviscid Interaction

Viscous effects were taken into account in an approximate fashion by coupling the three-dimensional Euler equations with the two-dimensional compressible turbulent inverse integral boundary-layer equations. The inverse boundary-layer method is described in Ref. 15. An inverse method allows for regions of separated flow and the one described in Ref. 15 can be used everywhere, whether or not the flow separates.

Viscous-inviscid interaction solutions were obtained using the surface source method as ex-

plained in Refs. 16 and 17. This method accounts for interaction by imposing a surface source term in each of the Euler equations as described in Ref. 18. The iteration procedure used in Ref. 17 was followed except that the boundary-layer equations were solved after every 20 time cycles of the Euler equations rather than after every 50 cycles. The reason for this is that the time step resulting from the present three-dimensional grid (96 x 16 x 16) was larger than that resulting from the finer two-dimensional grid (128 x 30) used in Ref. 17. Both the inviscid and viscous-inviscid interaction solutions involved 400 Euler equation cycles. Carter's method[19] of iterating on the displacement thickness was used, with a relaxation of unity.

Boundary-layer solutions were obtained over the wing in the freestream direction at each spanwise location. Ten cells in the spanwise direction were taken on the wing. The boundary-layer solutions were started at each span station at the 20 percent local chord location on the lower surface and the 15 percent local chord location on the upper surface, as this corresponded to the boundary-layer trip locations used in the experiment.[12]

## V. Results and Comparisons

Available experimental transonic data appear to be those of Wedge and Crowder.[12] This experiment was stated [12] to be of an exploratory nature to identify order-of-magnitude slipstream-wing interaction effects and not to establish highly accurate results. A simulator consisting of a high pressure air driven ejector system was used to simulate a modern prop-fan slipstream. A schematic of the simulator and wing is shown in Fig. 2. The simulator exit diameter was 11.7 percent of the model span. The airfoil sections defining the wing are tabulated in Ref. 12. This wing had 32° of quarter chord sweep and a taper ratio of 0.30.

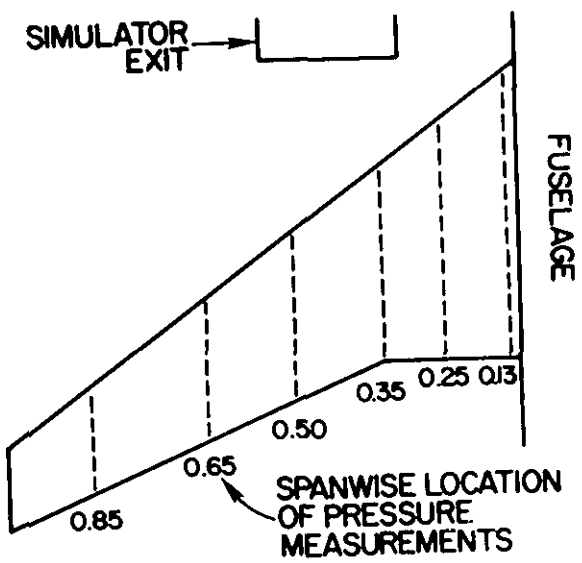


Fig. 2 Schematic of Simulator and Wing

All numerical solutions were obtained on a 96 x 16 x 16 C-type grid with 60 points on the wing at each of 11 span locations. The experiment used a wing-body combination; however, the grid was for a wing alone. Moreover, for these initial computations no special gridding of the propeller was used. The propeller (or simulator) region was, therefore, essentially a rectangle in appearance when viewed from directly upstream or downstream. The C-type grid did permit a reasonably vertical simulation of the propeller region.

An example of viscous-inviscid interaction results compared to purely inviscid results is given in Fig. 3 for $M_\infty$ (freestream Mach number) of 0.80, Re (Reynolds number based on mean aerodynamic chord) of $2.3 \times 10^6$, $\alpha$ (angle of attack) of 1.83°, $\eta$ (semispan location) or 0.65, and no propeller simulator. As illustrated in Fig. 3, viscous-inviscid interaction improves the agreement between the numerical and experimental results by moving the shock location forward and decreasing the lift in general. However, this grid is not sufficiently fine, particularly over the aft portion of the wing where the grid spacing approaches 6 percent of the local chord, to resolve the shock adequately. The discrepancy on the aft portion of the lower surface exists in all comparisons. This may be an indication that three-dimensional boundary-layer effects, not included in these computations, are important.

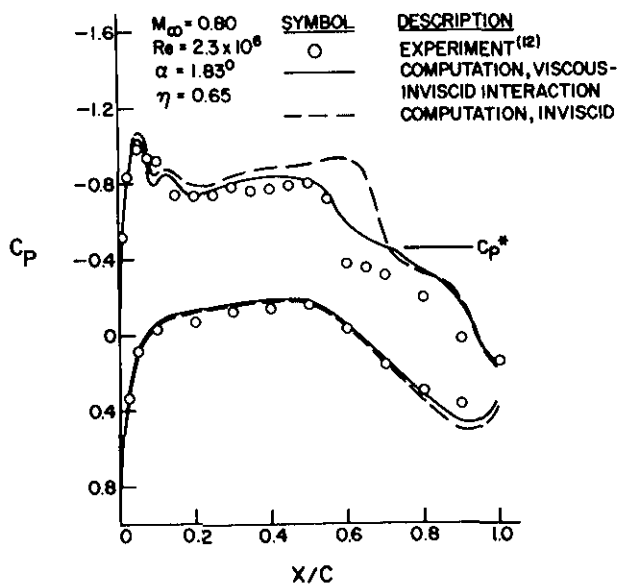


Fig. 3 Numerical and Experimental Wing Surface Pressures With No Simulator and With and Without Viscous Effects

Comparisons of numerical and experimental wing surface pressures with and without the simulator, and with and without the swirl are given in Fig. 4 for $M_\infty$ = 0.70 and $\alpha$ = 3°. The term $\Delta P_{T_J}$ is the jump in total pressure at the simulator. Results are presented at two span locations, $\eta$ = 0.35 and $\eta$ = 0.50. These span locations were selected because the propeller simulator has the greatest influence on the flow about the wing at these locations (see Fig. 2). Figures 4a and 4b indicate that the propeller simulator changed the wing

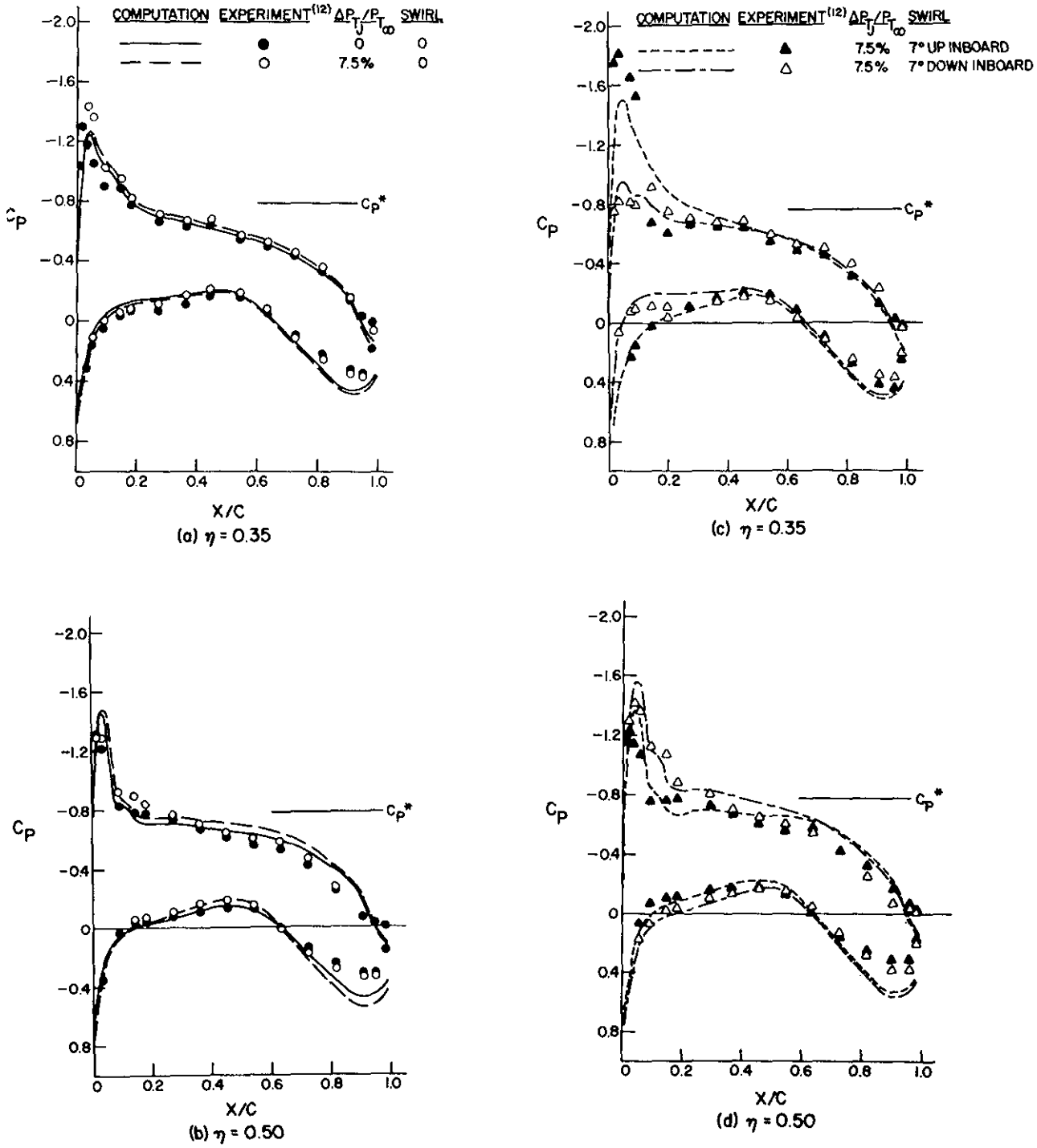


Fig. 4 Numerical and Experimental Wing Surface Pressures With and Without Simulator for $M_\infty = 0.70$, $Re = 2.3 \times 10^6$, and $\alpha = 3°$

pressure distribution somewhat compared to no simulator. However, Figs. 4c and 4d indicate that swirl, both up inboard and down inboard, has a much larger effect. Swirl influences the pressure distribution more on the inboard station ($\eta = 0.35$) than the outboard station ($\eta = 0.50$). The computations in Fig. 4 include viscous-inviscid interaction, and are considered to be in reasonable agreement with the experimental data.

Numerical and experimental span load distributions are presented in Fig. 5 for $M_\infty = 0.80$ and $\alpha = 3°$. The span load paramenter used in Fig. 5, $cc_\ell/c_{mac}$, is the local lift coefficient $c_\ell$ times the ratio of the local chord c to the mean aerodynamic chord $c_{mac}$. The most interesting results are those which include swirl. Quantitative agreement between theory and experiment is worse on the outboard portion of the wing although the numerical results are in good qualitative agreement with the experimental data in Fig. 5. The computations include viscous-inviscid interaction.

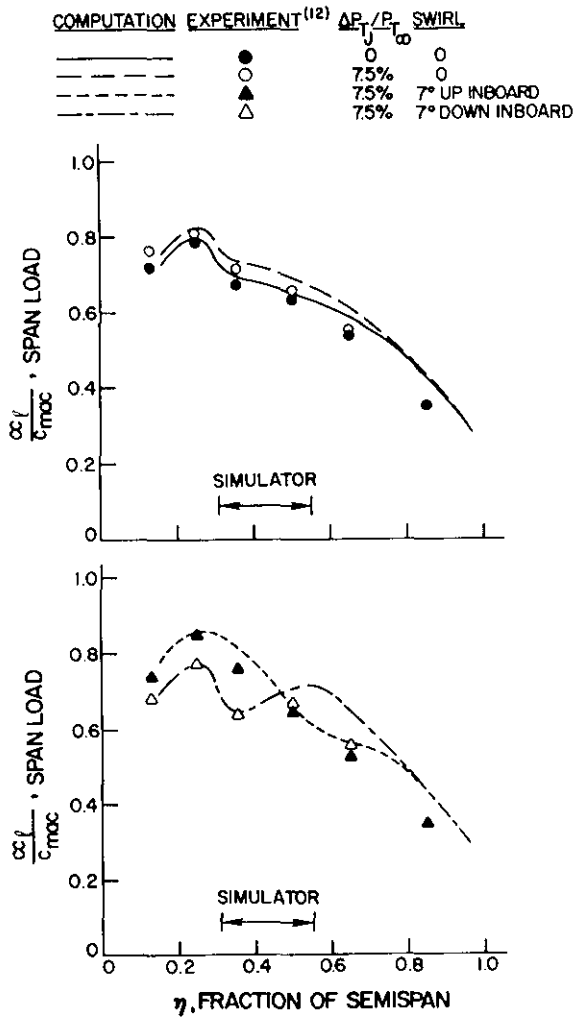


Fig. 5 Numerical and Experimental Spanwise Load Distributions for $M_\infty = 0.80$, $Re = 2.3 \times 10^6$, and $\alpha = 3°$

The influence of the propeller simulator on the upper wing surface boundary layer for $M_\infty = 0.80$ and $\alpha = 3°$ is illustrated in Fig. 6. Of particular interest is whether or not flow separation occurs as a consequence of the propeller slipstream. Although the boundary-layer treatment is two-dimensional, the inverse method used can predict separated flow. The local skin friction coefficient, $c_f$, is plotted in Fig. 6 at $\eta = 0.43$ which is the wing span station located downstream of the center of the propeller simulator. The influence of 7° down inboard swirl as compared to 7° up inboard swirl is to strengthen the upper surface shock and move it aft somewhat. Although the flow does not separate in the computations with swirl in either direction, the upper surface boundary layer corresponding to the case with 7° down inboard swirl is close to separation just downstream of the shock and near the trailing edge due to the stronger shock.

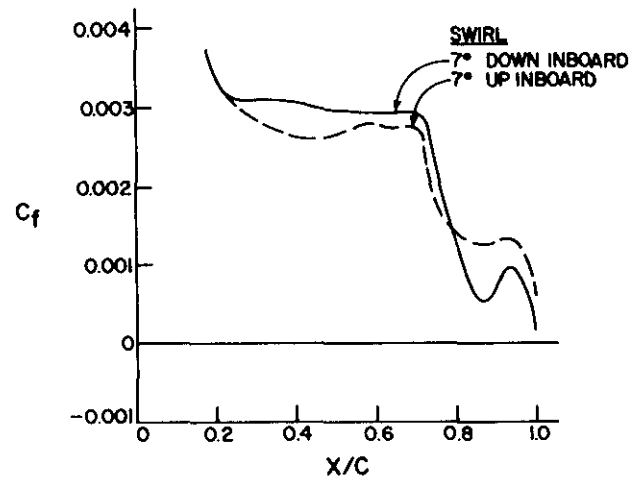


Fig. 6 Influence of Swirl on the Upper Surface Wing Boundary Layer at $\eta = 0.43$ for $M_\infty = 0.80$, $Re = 2.3 \times 10^6$, and $\alpha = 3°$

Experimental incremental lift coefficients are presented in Ref. 12 for various simulator to freestream total pressure ratios ($P_{T_J} / P_{T_\infty}$), freestream Mach numbers and up inboard swirl angles. The lift increments are referenced to $P_{T_J}/P_{T_\infty} = 1.000$ and zero swirl. Computations for simulator to freestream Mach numbers of 0.70 and 0.80, and swirl angles of zero and 7° up inboard are compared with experimental data in Fig. 7. The computed incremental lift results with viscous-inviscid interaction are shown in Fig. 7 to be in good agreement with the experimental data.

## VI. Conclusions

A computational method was presented for solving the three-dimensional time-dependent Euler equations with force terms which are similar to body forces. These particular force terms were introduced to simulate a propeller. In addition, viscous effects were accounted for in an approximate fashion by coupling the three-dimensional Euler equations with the two-dimensional compressible

turbulent inverse integral boundary-layer equations.

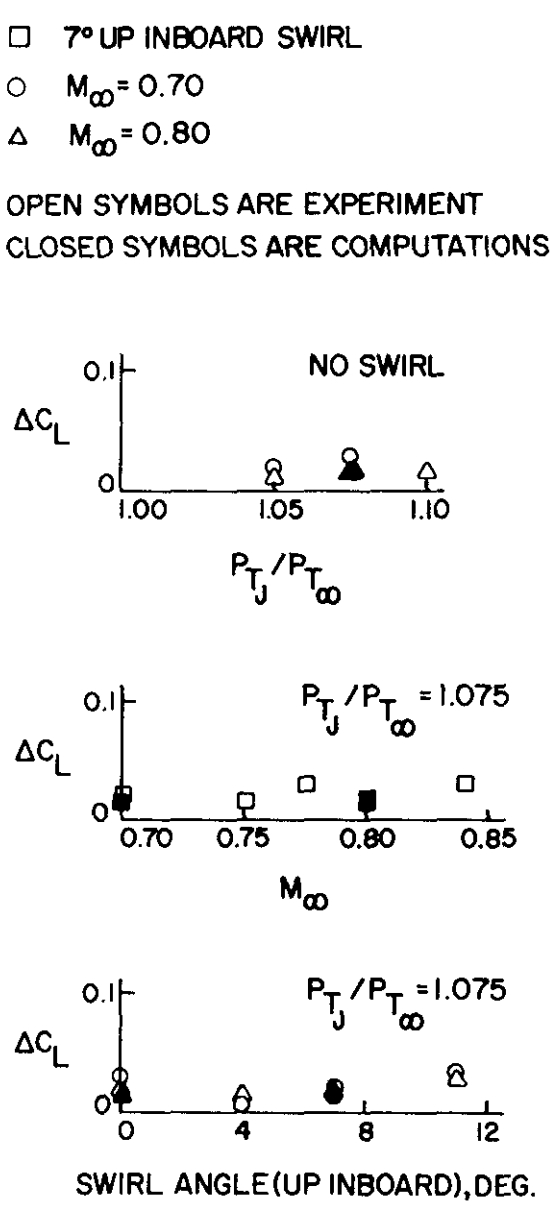


Fig. 7 Numerical and Experimental Incremental Lift Data for $\alpha = 3°$ and $Re = 2.3 \times 10^6$

Viscous-inviscid interaction computations were carried out for transonic flow about a 32° swept supercritical wing with: (1)no influence of a propeller, (2)the influence of a propeller producing thrust only, and (3)the influence of a propeller producing both thrust and swirl (in either direction). Although a wing with only one propeller was investigated, there is no restriction on the number of propellers that can be included, nor the direction of swirl produced by each propeller. The 96 x 16 x 16 grid used was rather coarse; however, comparisons with experiments indicate the computational method is a useful tool for investigating this practical three-dimensional flow problem with vorticity.

All computations were performed on a CRAY-1S computer that had about 900,000 words of available memory. A viscous-inviscid interaction solution on a 96 x 16 x 16 grid with 400 Euler equation cycles and 20 boundary-layer equation cycles required 341 seconds and the 900,000 words of memory.

## References


(1) Chow, F., Krause, E., Liu, C. H., and Mao, J. "Numerical Investigations of an Airfoil in a Non-Uniform Stream," Journal of Aircraft, Vol. 7 No. 6, 1970, pp. 531-537.

(2) Kleinstein, G. and Liu, C. H., "Application of Airfoil Theory for Nonuniform Streams to Wing Propeller Interaction," Journal of Aircraft, Vol. 19, No. 2, 1972, pp. 137-142.

(3) Lan, C. E., "Wing-Slipstream Interaction with Mach Number Nonuniformity," Journal of Aircraft, Vol. 12, No. 10, 1975, pp. 759-760.

(4) Shollenberger, C. A. "Three-Dimensional Wing/Jet Interaction Analysis Including Jet Distortion Influences," Journal of Aircraft, Vol. 12, No. 9, 1975, pp. 706-713.

(5) Ting, L., Lin, C. H., and Kleinstein, G., "Interference of Wing and Multipropellers," AIAA Journal, Vol. 10, No. 7, 1972, pp. 906-914.

(6) Boctor, M. L., Clay, C. W., and Watson, C. F., "An Analysis of Prop-Fan/Airframe Aerodynamic Integration," NASA CR-152186, October 1978.

(7) Rizk, M. H., "Propeller Slipstream/Wing Interaction in the Transonic Regime," Flow Research Report No. 132, Kent, Washington, June 1979.

(8) Narain, J. P., Unpublished Internal Lockheed Report, November 1981.

(9) Jeffrey, A. and Taniuti, T., Non-Linear Wave Propagation. Academic Press, New York, 1964.

(10) MacCormack, R. W., and Paullay, A. J., "The Influence of the Computational Mesh on Accuracy for Initial Value Problems with Discontinuous or Nonunique Solutions," Computers and Fluids, Vol. 2, 1974, pp. 339-361.

(11) Shercliff, J. A., A Textbook of Magnetohydrodynamics. Pergamon Press, New York, 1965.

(12) Wedge, H. R. and Crowder, J. P., "Simulated Propeller Slipstream Effects on a Supercritical Wing," NASA CR-152138, June 1978.

(13) Jameson, A., Schmidt, W., and Turkel, E., "Numerical Solution of the Euler Equations by Finite Volume Methods Using Runge-Kutta Time Stepping Schemes," AIAA Paper No. 81-1259, June 1981.

(14) Rizzi, A., "Numerical Implementation of Solid Body Boundary Conditions for the Euler Equations," ZAMM, Vol. 58, 1978, pp. 301-304.

(15) Whitfield, D. L., Swafford, T. W., and Donegan, T. L., "An Inverse Integral Computational Method for Compressible Turbulent Boundary Layers," in Transport Phenomena in Fluid Mechanics, Springer-Verlag, Berlin, 1982.

(16) Whitfield, D. L., Swafford, T. W., and

Jacocks, J. L., "Calculation of Turbulent Boundary Layers with Separation and Viscous-Inviscid Interaction," AIAA Journal, Vol. 19, No. 10, October 1981, pp. 1315-1322.

(17)

Schmidt, W., Jameson, A., and Whitfield, D., "Finite Volume Solutions to the Euler Equations in Transonic Flow," AIAA Journal, Vol. 20, 1982.

(18)

Whitfield, D., Thomas, J., Jameson, A., and Schmidt, W., "Computation of Transonic Viscous-Inviscid Interacting Flow," Second Symposium on Numerical and Physical Aspects of Aerodynamic Flows, Long Beach, CA, January 1983.

(19)

Carter, J. E., "A New Boundary-Layer Inviscid Iteration Technique for Separated Flow," AIAA Paper No. 79-1450, July 1979.